SURFACE ROUGHNESS STUDY OF HIGH-SPEED RAILWAY WHEEL MATERIALS BASED ON LASER-INDUCED BREAKDOWN SPECTROSCOPY

Aiguo Ouyang*, Bin Yu, Jun Hu, Tongzheng Lin, Yande Liu

School of Mechanical & Electrical Engineering, East China Jiaotong University, Nanchang, China; e-mail: ouyang1968711@163.com

An experimental platform of laser-induced breakdown spectroscopy (LIBS) is used to obtain the spectral information of seven ER8 high-speed train wheel samples with different surface roughnesses; the correlations between their spectral line intensities and the ratios of spectral line intensities to the surface roughnesses of the samples are investigated. The results show that the spectral line intensities of the base element Fe and the alloying elements Cr, Mo, and V, the intensity ratios of ion lines to atomic lines, and the spectral line intensity ratios of alloying elements to base elements are all correlated with the surface roughnesses of the samples to different degrees. In addition, random forest (RF) models with spectral line intensities and spectral line intensities with spectral line intensity ratios as variables are established using the correlations. The study shows that it is feasible to qualitatively analyze the surface roughnesses of high-speed railway wheel materials using laser-induced breakdown spectroscopy with an RF algorithm; this technique can be used to measure and evaluate the surface roughnesses of wheels in the field and provide some basis for the application of LIBS technology to the study of high-speed railway wheels with different surface roughnesses.

Keywords: *laser-induced breakdown spectroscopy, high-speed train wheel material surface roughness, spectral line intensity, random forest.*

ОПРЕДЕЛЕНИЕ ШЕРОХОВАТОСТИ ПОВЕРХНОСТИ МАТЕРИАЛОВ ВЫСОКОСКОРОСТНЫХ ЖЕЛЕЗНОДОРОЖНЫХ КОЛЕС НА ОСНОВЕ ЛАЗЕРНО-ИСКРОВОЙ ЭМИССИОННОЙ СПЕКТРОСКОПИИ

A. Ouyang*, B. Yu, J. Hu, T. Lin, Y. Liu

УДК 543.422

Школа механики и электротехники Восточно-Китайского университета Цзяотун, Наньчан, Китай; e-mail: ouyang1968711@163.com

(Поступила 4 апреля 2022)

С помощью лазерно-искровой эмиссионной спектроскопии (LIBS) получена спектральная информация для семи образцов колес высокоскоростных поездов ER8 с различной шероховатостью поверхности. Исследованы корреляции между интенсивностью спектральных линий, их отношением и шероховатостью поверхности образцов. Показано, что интенсивности спектральных линий основного элемента Fe и легирующих элементов Cr, Mo и V, отношения интенсивностей ионных линий к атомным линиям и отношения интенсивностей спектральных линий легирующих элементов к основным элементам коррелируют с шероховатостью поверхности образцов в разной степени. Модели случайного леса (RF) с интенсивностями спектральных линий и отношениями интенсивностей спектральных линий в качестве переменных использованы для корреляций. Проанализирована шероховатость поверхности материалов высокоскоростных железнодорожных колес с использованием LIBS и алгоритма RF. Метод можно использовать для измерения и оценки шероховатости поверхности колес в полевых условиях, обеспечив основу для применения LIBS при исследовании колес высокоскоростных железных дорог с различной шероховатостью поверхности.

Ключевые слова: *лазерно-искровая эмиссионная спектроскопия, шероховатость поверхности материала колеса высокоскоростного поезда, интенсивность спектральной линии, модель случайного леса.*

Introduction. In recent years, the high-speed railroad, with its speed, convenience, comfort, and efficiency, has developed rapidly in China, gradually forming a four vertical and four horizontal network basis; the goal for the high-speed railroad network is to exhibit an eight vertical and eight horizontal framework [1–3]. With the rapid development of domestic high-speed trains, the operating speed has continuously improved, and the recent high-speed trains run at speeds of 300 km/h or more on the mainline. By the end of 2021, China's high-speed railroad mileage exceeded 40,000 km, ranking first in the world; it is expected that by 2030, China's high-speed railroad mileage will reach 45,000 km [4, 5]. With the rapid growth in the total operational mileage of high-speed railroads, service safety is receiving increasing attention. The safety of high-speed wheels, as a key running part of high-speed rails, directly affects the operation of trains [6, 7]. The train's traction operation, braking, and deceleration all rely on wheel–rail friction to provide traction and braking force, and the contact quality between the wheels and rails directly affects the train's safety in service. Under the wheel–rail friction actions of rolling contact and multiaxis alternating stress, wheel–rail materials produce different degrees of wear and rolling contact fatigue after a period of service, which affects the flatness and smoothness of the wheel–rail tread in subtle cases and the smooth operation of trains in severe cases [8]. Surface roughness, as one of the most important indicators for evaluating wheel performance, not only influences the wear mechanism of the wheel material but also affects its wear resistance. In general, the lower the surface roughness, the smoother the wheel surface and the better the wear resistance [9, 10].

The measurement of surface roughness of a high-speed railway wheel material is important for evaluating the wheel performance; however, the traditional measurement method for surface roughness is less efficient and has certain limitations, making it unsuitable for large-scale, long-term measurements and high-precision workpiece surface measurements. As an emerging elemental measurement technique, laser-induced breakdown spectroscopy (LIBS) can quickly detect samples; it has the advantage of real-time online measurement, and it causes less damage to samples. LIBS is widely used in biomedical, mineral, environmental pollution, and food safety applications, among others [11–20]. In recent years, the use of the LIBS technique to detect the surface roughness of samples has been proposed. Cabalin et al. [21] conducted a laser ablation study on stainless steel samples with different surface roughnesses and found a correlation between the LIBS signal of a single pulse and the surface roughness of the sample under low laser energy conditions. Rauschenbach et al. [22] proposed that rocks and soils with different roughnesses could be distinguished by the characteristic spectra of LIBS signals. Rapin et al. [23] analyzed the roughnesses of Martian rocks using LIBS and found that the roughness of the sample significantly affected the H signal in the LIBS spectrum, whereas the other emission lines in the spectrum were not affected. Wang et al. [24] investigated the effects of the laser ablation of carbon steels with different surface roughnesses at diameters of approximately 10 μm on the spectral stability and quantitative analysis capability, and found that the effect of the surface roughness of the sample on the spectral stability was negligible when the relative height of the sample surface was certain; in addition, the effect of the surface roughness of the sample on the quantitative analyses of manganese, silicon, nickel, vanadium, chromium, and copper in carbon steel were negligible when the internal standard method of the Fe spectrum was used under specific conditions. Chen et al. [25] studied the effect of the surface roughness of silicone rubber on the LIBS signal and found that there were good correlations between the sample roughnesses and the spectral line intensities of each subject element; however, the correlations between the characteristic spectral line intensities and the atomic line intensity ratios of different subject elements and the sample roughnesses were not obvious.

To date, there is no reported research on LIBS technology for the surface roughness inspection of wheel materials. Given the characteristics of LIBS, such as rapid detection and real-time online measurement, a method of identifying samples with different surface roughnesses using LIBS technology with wheel materials as the target is proposed in this study. The correlations between the spectral line characteristics and the surface roughnesses of the samples are analyzed to provide a basis for the application of LIBS technology to the study of high-speed railway wheels with different surface roughnesses.

Experiment. *Sample preparation.* The ER8 steel studied in this experiment has excellent wear resistance, moderate hardness, and strength, which can adapt to the complex environment of high-speed train service, and it has comprehensive advantages in terms of safety; thus, it is widely used in the wheels of high-speed trains in China [26]. The main chemical compositions of the samples are shown in Table 1. There were seven cylindrical samples used in this study, with diameters of 20 mm and heights of 10 mm. The untreated original sample was labeled sample no. 1, and five other original samples were polished with 60-, 120-, 800-, 1200-, and 2000-mesh sandpaper until the scratches were consistent; then, the samples were cleaned with anhydrous ethanol and numbered as samples Nos. 2, 3, 4, 5, and 6, respectively. A sample was

polished with a diamond suspension with a 3-μm particle size after being ground with 2000-mesh sandpaper, polished to a mirror surface, cleaned with anhydrous ethanol to remove the surface oxide layer, and finally labeled sample No. 7. A white light interferometer model Rtec UP-Sigma was used to measure the surface roughnesses of samples with different surface treatments. Five equally spaced line segments were marked on the surface of each sample, the surface roughness was measured on each line segment using the white light interferometer, and the average of the roughnesses measured on the five-line segments was taken as the surface roughness value of the sample. The measurement results are shown in Table 2. Figure 1 shows the surface appearance of the samples with different surface treatments after 100 times magnification by a metallographic microscope.

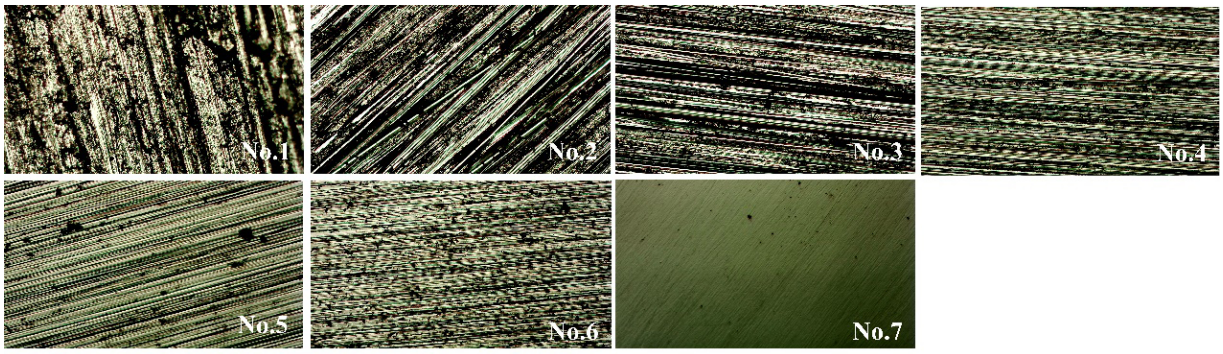

Fig. 1. Surface samples of different roughness values.

TABLE 1. Main Chemical Composition of ER8 Steel (wt.%)

Element	Mass fraction, %	Element	Mass fraction, %
Cr	2.43	Si	0.32
Mo	2.02	Ni	0.03
Mn	1.27	P	0.012
V	0.98	S	0.003
C	0.35		

TABLE 2. Surface Roughness Values of the Samples

Number	Surface treatment	Roughness measurements, μm					Average surface roughness value, μm
		1	2	3	4	5	
1	Raw material	5.952	5.289	4.769	5.703	5.963	5.535
2	60# sandpaper	1.783	1.708	1.888	1.560	1.690	1.726
3	120# sandpaper	1.110	0.976	0.968	0.996	0.933	0.997
4	800# sandpaper	0.180	0.174	0.173	0.176	0.181	0.177
5	1200# sandpaper	0.055	0.058	0.069	0.059	0.062	0.061
6	2000# sandpaper	0.041	0.036	0.040	0.038	0.033	0.038
7	3-μm diamond suspension	0.030	0.025	0.020	0.019	0.030	0.025

LIBS. The equipment model used in the experiment was Ocean Optics MX2500+, and the LIBS system schematic is shown in Fig. 2. The laser used was a solid-state Nd:YAG laser (Quantel, Big Sky Laser Ultra50), which produced an optical excitation of 1060 nm with a laser energy setting of 50 mJ, a laser pulse duration of 8 ns, and a power density of 1.99×10^{10} W/cm^2 of laser radiation in the impact spot. The incident laser was reflected and focused vertically onto the sample surface by a lens with a focal length of 75 mm to produce plasma. The accompanying spectral information was collected by an optical fiber and transmitted to a five-channel multichannel spectrometer, where the wavelength and signal intensity values of the elements were collected by setting the relevant parameters with the MaxLIBS software that accompanied the spectrometer. The spectrometer had a wavelength range of 198.71 to 727.69 nm, a spectral resolution of 0.1 nm, and a spectral integration time of 1 ms. The delay time was set to 2500 ns based on the optimal signal-to-

noise ratio. Each sample was measured with a single laser pulse at 25 different locations, and the experimental data from the single laser pulse were used as one measurement sample. This finding indicated that there were seven samples, each with 25 subsamples, for a total of 175 experimental samples; the average of the spectral data from the 25 subsample measurements was used as the spectral data value corresponding to the surface roughness of that sample.

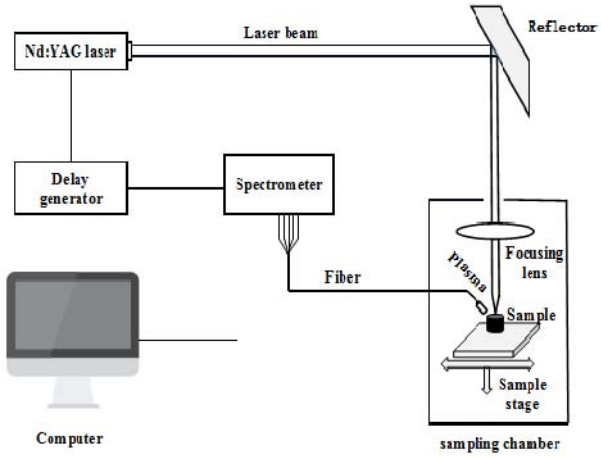

Fig. 2. Schematic diagram of the LIBS system.

Data processing. In addition to the chemical information of the sample itself, the spectrum contained other irrelevant information and noise. To reduce the influences of the fluctuation of the laser energy, the difference in the resolution of the spectrometer, the difference in the external environment, and the inhomogeneity of the sample, spectral preprocessing of the LIBS spectral data was performed [27]. Three preprocessing methods – baseline, multiplicative scatter correction (MSC) and standard normal variate transformation (SNV) – were used to preprocess the model before building it; then, the model was built by combining the preprocessed model with the RF algorithm.

The baseline, also known as background removal, tended to have large fluctuations in LIBS spectral data owing to variations in laser energy, plasma formation conditions, instrumental electronic noise, and thermal noise effects. These aspects could add more baseline drift and background interference to the acquired spectral data, even masking the information of the material to be measured, thus greatly affecting the accuracy of the spectral analysis [28]. Parameter y is the spectral value obtained after baseline correction:

$$y = x - \min(x), \tag{1}$$

where x is all spectral values, min(x) is the minimum of all spectral values.

MSC is a common algorithm used in spectral data preprocessing, mainly to eliminate the scattering effects of sample particle size, thickness, and surface inhomogeneities caused by the sample preparation process, and it is often used in solid diffuse reflectance and liquid transmission spectral data preprocessing [29]. This phenomenon was achieved as follows:

The spectra of all experimental samples were averaged to obtain $\bar{x}$ (the ideal spectrum).

The spectra of each sample were subjected to a one-dimensional linear regression against the mean spectrum, and a least squares problem was solved to obtain the baseline shift b_0 and offset b for each sample:

$$x = b_0 + \bar{x}b. \tag{2}$$

The spectrum of each sample was corrected; the resulting baseline shift b_0 was subtracted and divided by the offset b to obtain the corrected spectrum:

$$x_{\mathrm{MSC}} = (x - b_0)/b. \tag{3}$$

SNV is generally used to mitigate the effects of nonspecific scattering on spectral data due to sample particle size, thickness, and surface heterogeneity caused by improper handling during sample preparation; it could be used to address various issues, such as baseline drift and tilt effects [30]. The formula is below:

$$X_{i,\mathrm{SNV}} = (X_{i,k} - \overline{X_i}) \Bigg/ \sqrt{\frac{\sum_{k=1}^{m} (X_{i,k} - \overline{X_i})^2}{(m-1)}}, \tag{4}$$

where $\bar{X}_i$ is the average of the ith spectrum, i = 1, 2, …, n, and n are the number of samples, k = 1, 2, …, m, where m is the wavelength.

Random forest (RF) is an algorithm that uses the idea of integrated learning to integrate multiple decision trees in the field of machine learning and is essentially a classifier. Random forests are composed of multiple decision trees, and their final classification results are determined by the combined votes of multiple decision trees. The construction process was as follows. A subset of n data is randomly drawn from the original sample set; then, the subsets of data were used to construct subdecision trees and obtain more decision trees after several cycles. The data were placed into each subdecision tree and one result was output per subdecision tree. The qualitative problem generated classification results by voting, and the quantitative problem used the mean of n model predictions as the final prediction result. Relative to individual classifiers, the RF algorithm has better classification results and could effectively improve the generalization ability of a learning system [31].

Results and discussion. *Spectral characterization.* A representative spectrum of sample No. 1 within the wavelength range 200–500 nm is shown in Fig. 3, from which a large number of characteristic spectral lines of the matrix elements (Fe) and alloying elements (Cr, Mo, and V) can be clearly discerned.

To analyze the differences between samples with different surface roughnesses and the characteristics of laser ablation plasma spectra, the spectral intensities of the matrix element Fe and the alloying elements Cr, Mo, and V are analyzed separately for samples with different surface roughnesses; Fe I 373.71316 nm, Cr I 360.532 nm, Mo I 319.3979 nm, and V I 370.3574 nm characteristic spectral lines are selected as the objects

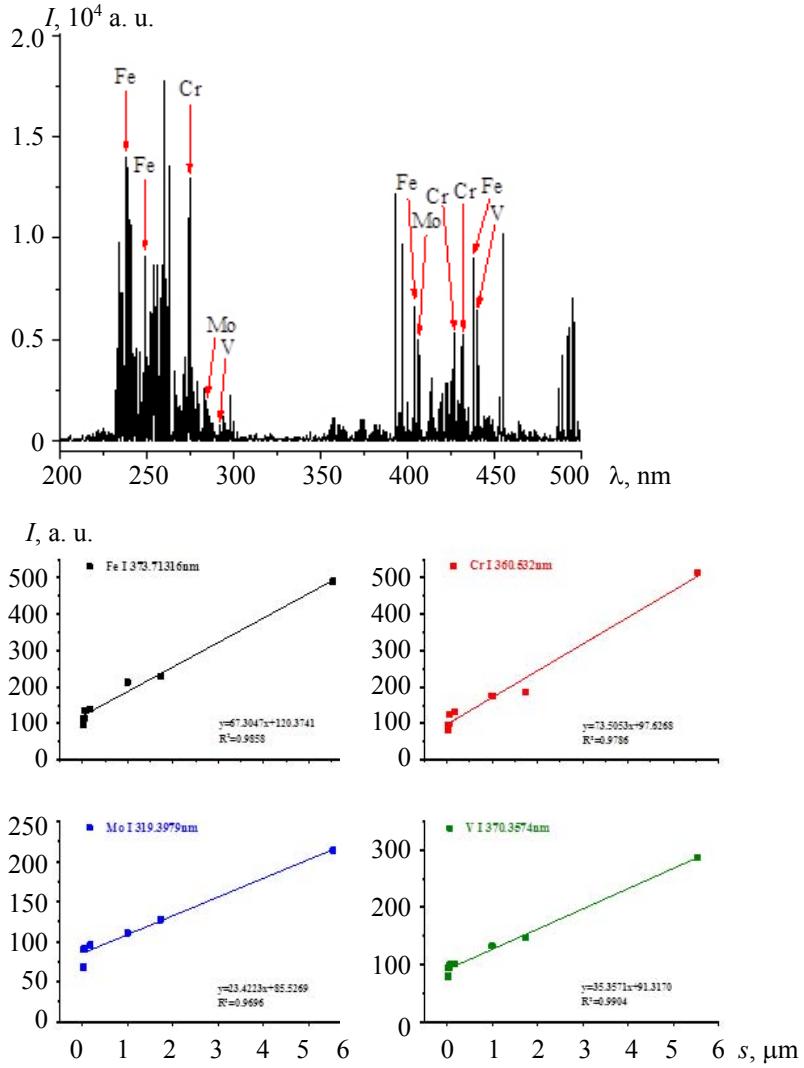

Fig. 3. Representative spectra of sample No. 1 and relationship between the surface roughnesses and the spectral line strengths of different elements in the sample.

of study for analysis. As shown in Fig. 3, the spectral line intensities of Fe, Cr, Mo, and V elements all have different degrees of positive correlation with the surface roughnesses of the samples owing to the different excitation characteristics and self-absorption effects of different elements; thus, the slopes of the spectral line intensities of different elements are distinct. The change in surface roughness of the sample affects the absorption process of the laser by the material and thus the subsequent laser-plasma state, which can better reflect the differences between samples with different surface roughnesses. In addition, the correlations among the intensity ratios of ion lines to atomic lines, the spectral intensity ratios of alloying elements to matrix elements, and the surface roughness of the samples with different surface roughnesses are analyzed experimentally. According to the chemical properties, excitation potential, ionization degree, and spectral intensity characteristics of different elements, the following spectral lines are selected for analysis: Fe I 373.71316 nm, Fe II 249.32637 nm, Cr I 360.532 nm, Cr II 206.546 nm, Mo I 315.8167 nm, and V I 318.3992 nm.

As shown in Fig. 4a,b, the intensity ratios of (Fe II 249.32637 nm/Fe I 373.71316 nm), (Cr II 206.546 nm/Cr I 360.532 nm) have negative correlations with the surface roughnesses of the samples to different degrees; this result shows that the intensity ratios of ion lines to atomic lines can be used to reflect the matrix characteristics of the sample. Additionally, the same trend is mapped in the ratios of ionization and recombination phenomena occurring in Fe and Cr particles in the plasma as the surface roughness of the sample increases. As shown in Fig. 4c,d, the spectral intensity ratios of (Mo I 315.8167 nm/Fe I 373.71316 nm), (V I 318.3992 nm/Fe I 373.71316 nm) are correlate to varying degrees with the surface roughnesses of the samples; this finding indicates that the matrix effect is different when the laser acts on the object with different matrix characteristics, and the ratios of the spectral intensities of the alloy element and the matrix element can be used to reflect the matrix characteristics of the sample. From the above, it can be concluded that the spectral intensity ratios of the matrix elements, alloying elements, and ion lines to atomic lines and the spectral intensity ratios of alloying elements to matrix elements of the sample can characterize the surface roughness of the sample material to some extent.

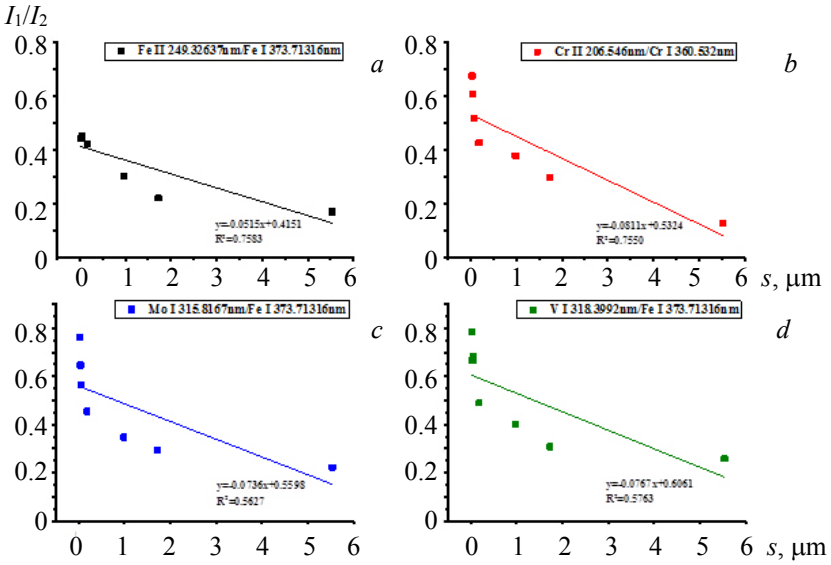

Fig. 4. Relationship between the spectral intensity ratios of alloying elements and matrix elements and the surface roughness of the sample: (a) (Fe II 249.32637 nm/Fe I 373.71316); (b) (Cr II 206.546 nm/Cr I 360.532 nm); (c) (Mo I 315.8167 nm/Fe I 373.71316 nm); (d) (V I 318.3992 nm/Fe I 373.71316 nm).

Model establishment using spectral line intensity. To qualitatively analyze the surface roughnesses of the samples, three preprocessing methods – baseline, MSC, and SNV – are used to preprocess the spectral intensity of the full waveband, and then the RF algorithm is used to establish a qualitative model. The accuracy of the model is experimentally evaluated by the accuracy of the rate of model discrimination (Fig. 5). Samples with surface roughness values of 5.535 and 1.726 μm are artificially set as category 0, samples with surface roughness values of 0.997 and 0.177 μm are set as category 1, and samples with surface roughness values of 0.061, 0.038, and 0.025 μm are set as category 2. The model is divided into a modeling set and a prediction set in a 2:1 ratio, with 116 samples in the modeling set and 59 samples in the prediction set.

The results of the evaluation indices of the model are shown in Table 3; the results show that the RF model built after SNV preprocessing has the best effect. The number of its prediction set misclassification is 7, and the model accuracy is 88.1%.

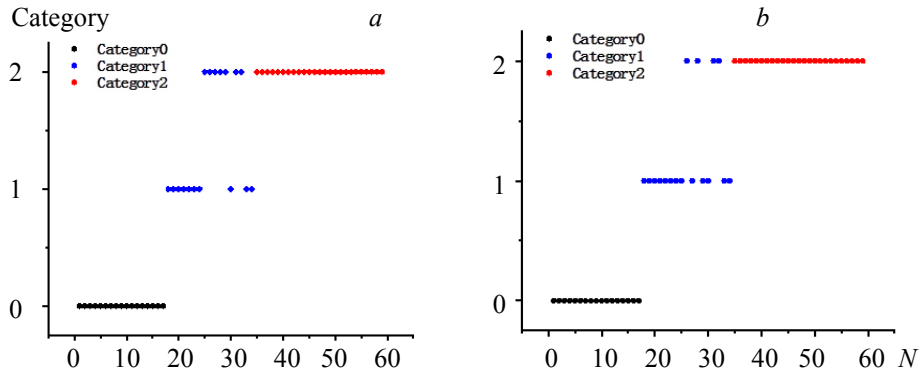

Fig. 5. Effect of the RF model built after SNV preprocessing of the full-band spectral line intensity (a) and of the spectral intensity combined with the spectral intensity ratio data (b).

TABLE 3. Model Evaluation Index Results (Variable is Intensity)

Pretreatment method	Method	Misjudgment times/piece	Discrimination accuracy, %
None	RF	10	83.1
Baseline		10	83.1
MSC		8	86.4
SNV		7	88.1

The model is established by using the spectral line intensity combined with the spectral line intensity ratio. In the above study, the model built using the spectral line intensity as a variable obtains acceptable results, but the number of misjudgments in the model prediction set is excessive. To further optimize the model, the intensity ratios of ion lines to atomic lines (II/I) and the spectral intensity ratios of alloying elements to matrix elements (A/M) are considered to reflect the matrix characteristics of the sample; the spectral intensity and spectral intensity ratio are combined to build a qualitative model. Seventy six spectral lines of the matrix and alloying elements without mutual interference phenomena that are clearly distinguished are selected by hand, as shown in Table 4.

TABLE 4. Spectral Lines of Manually Selected Matrix Elements and Alloying Elements

Spectral line type	Spectral wavelength, nm
Fe I	248.3271, 248.8143, 249.0644, 252.2849, 271.9027, 278.8105, 344.0606, 358.1193, 371.9935, 373.4864, 373.7132, 374.5561, 374.9485, 375.8233, 382.0425, 285.9911, 404.5813, 438.3545
Fe II	234.3495, 238.2038, 239.5625, 240.4886, 249.3264, 258.5876, 259.8369, 260.7087, 261.1874, 273.9547, 274.9322, 275.5737
Cr I	357.8682, 359.3481, 360.532, 425.4331, 427.4806, 428.9733, 520.4505
Cr II	205.559, 206.154, 206.546, 267.716, 276.258, 276.655, 283.563, 284.324, 285.567, 286.51
Mo I	313.2594, 315.8167, 317.0344, 319.3979, 320.8839, 344.7124, 379.8252, 386.4104, 390.2953, 406.9882, 418.8324, 441.1695, 550.6494, 553.3031, 557.0444
V I	318.3412, 318.5385, 370.3574, 385.5845, 390.2256, 411.178, 411.518, 412.8064, 413.1989, 437.923, 438.998, 439.5223, 440.8195, 609.0208

TABLE 5. Model Evaluation Index Results (Variables are Intensities, II/I and A/M)

Pretreatment method	Method	Misjudgment times, piece	Discrimination accuracy, %
None	RF	9	84.7
Baseline		9	84.7
MSC		6	89.8
SNV		4	93.2

The intensity ratios of ion lines to atomic lines (II/I) and the spectral intensity ratios of alloying elements to matrix elements (A/M) are used to construct the spectral intensity ratio. As the response characteristics of different wavelength channels of the spectrometer are different, to reduce the influences of the differences in the response characteristics of the spectrometer in different wavelength ranges on the intensity ratios of the spectral lines, the spectral lines used to construct the intensity ratio are divided into three groups according to the spectrometer channels they are in 200–240 nm, 240–450 nm, and 455–660 nm; only the spectral lines within the same group are selected for pairwise combination to construct the intensity ratio variables of the spectral lines. Fe II 240.4886 nm is within the 240–450 nm range; thus, Fe II 240.4886 nm can only be paired and combined with Fe I spectral lines within the 240–450 nm range.

Three methods (baseline, MSC, and SNV) are used for preprocessing, and then the extracted feature bands are used to build the RF qualitative model. The model is still divided into a modeling set and a prediction set according to a 2:1 ratio, with 116 samples in the modeling set and 59 samples in the prediction set. Table 5 shows the results of the evaluation indices of the model; the results show that the model built with SNV preprocessing has the best effect, the number of misclassifications is 4, and the model accuracy is 93.2%. By comparing the models built with the spectral line intensities as variables, it can be found that the models built with the spectral line intensities combined with the spectral line intensity ratios are more effective, with fewer misevaluations, greater model accuracy, and improved model accuracy. The results show that using the spectral line intensity combined with the spectral line intensity ratio as an input variable can significantly improve the solution of the RF model for predicting the surface roughness of metallic materials; these findings indicate that the spectral line intensity ratio can be treated as the relative intensity of the spectral lines, which can reduce the influence of the fluctuation of the spectral signal caused by the instability of laser ablation [32, 33].

Conclusions. ER8 high-speed train wheel steel with different surface roughnesses was used as the research object, and spectral information was obtained using the LIBS technique. It was found that the spectral intensities of base element Fe and alloying elements Cr, Mo, and V, the intensity ratios of ion lines to atomic lines, and the intensity ratios of alloying elements to base elements, could correlate with the surface roughnesses of the samples to different degrees. RF models were established separately using different pretreatment methods with the spectral line intensities as variables; it was found that the model established after the SNV pretreatment had the best effect, with the number of misclassifications of the prediction set being 7 and the accuracy being 88.1%. To further optimize the model, the RF model was established by combining the spectral line intensities with the spectral line intensity ratios as input variables; it was found that the model established after SNV pretreatment had the best effect, the number of misjudgments in the prediction set was 4, and the accuracy rate was 93.2%. By combining the results of the analysis of the above model, it was found that the model established with the spectral line intensity combined with the spectral line intensity ratio as the input variable worked best. The study showed that it would be feasible to use laser-induced breakdown spectroscopy combined with an RF algorithm to qualitatively analyze the surface roughnesses of high-speed railway wheel materials, which could be used to measure and evaluate wheel surface roughnesses in the field to further predict the wheel performance and provide a certain guarantee of the safe operation of high-speed trains.

Acknowledgments. This work was supported by the National Natural Science Foundation of China (Grant No. 31760344), the Science and Technology Research Project of Jiangxi Provincial Education Department (GJJ60516), and Jiangxi Province Advantageous Science and Technology Innovation Team Construction Program Project (20153BCB24002).

REFERENCES

1. W. H. Zhang, *J. Rail and Rapid Transit*, **228**, No. 4, 367–377 (2014).
2. D. Wang, L. Wang, T. Chen, L. Lu, Y. Niu, A. L. Alan, *J. Geog. Sci.*, **26**, No. 12, 1725–1753 (2016).
3. G. Zhang, R. Ren, *Eng. Fail. Anal.*, **105**, 1287–1295 (2019).
4. J. Zhang, *EURASIP J. Wirel. Commun. Net.*, **2019**, No. 1, 1–8 (2019).
5. Z. Wang, J. Xu, Y. Wang, L. W. Wang, R. Z. Wang, *Appl. Therm. Eng.*, **188**, 116591 (2021).
6. Q. Zhang, Z. Zhu, J. Gao, G. Dai, L. Xu, J. Feng, *Acta Metall. Sin.*, **53**, No. 3, 307–315 (2016).
7. C. Lu, C. Cai, *Transp. Geotech.*, **25**, 100397 (2020).
8. L. M. Sweet, A. Karmel, R. Budell, D. Lassman, D. Schulte, *Veh. Syst. Dyn.*, **12**, No. 1–3, 177–178 (1983).
9. W. H. Ho, J. T. Tsai, B. T. Lin, J. Chou, *Expert Syst. Appl.*, **36**, No. 2, 3216–3222 (2009).
10. W. Grzesik, *J. Mater. Eng. Perform.*, **25**, No. 10, 4460–4468 (2016).
11. L. Radziemski, D. Cremers, *Spectrochim. Acta B: At. Spectrosc.*, **87**, 3–10 (2013).
12. V. K. Singh, V. Kumar, J. Sharma, *Lasers Med. Sci.*, **30**, No. 6, 1763–1778 (2015).
13. S. J. Rehse, H. Salimnia, A. W. Miziolek, *J. Med. Eng. Technol.*, **36**, No. 2, 77–89 (2012).
14. J. El Haddad, E. S. de Lima Filho, F. Vanier, A. Harhira, C. Padioleau, M. Sabsabi, A. Blouin, *Miner. Eng.*, **134**, 281–290 (2019).
15. Y. Bi, Y. Zhang, J. Yan, Z. Wu, Y. Li, *Plasma Sci. Technol.*, **17**, No. 11, 923 (2015).
16. Y. Zhang, T. Zhang, H. Li, *Spectrochim. Acta B: At. Spectrosc.*, **181**, 106218 (2021).
17. D. A. Gonçalves, G. S. Senesi, G. Nicolodelli, *Trends Environ. Anal. Chem.*, **30**, e00121 (2021).
18. D. Stefas, N. Gyftokostas, E. Nanou, P. Kourelias, S. Couris, *Molecules*, **26**, No. 16, 4981 (2021).
19. A. Velásquez-Ferrín, D. V. Babos, C. Marina-Montes, J. Anzano, *Appl. Spectrosc. Rev.*, **56**, No. 6, 492–512 (2021).
20. J. Huang, M. Dong, S. Lu, Y. Yu, C. Liu, J. H. Yoo, J. Lu, *Analyst*, **144**, No. 12, 3736–3745 (2019).
21. L. M. Cabalin, D. Romero, J. M. Baena, J. J. Laserna, *Surf. Interface Anal.*, **27**, No. 9, 805–810 (1999).
22. I. Rauschenbach, V. Lazic, S. G. Pavlov, H. W. Hübers, E. K. Jessberger, *Spectrochim. Acta B: At. Spectrosc.*, **63**, No. 10, 1205–1221 (2008).
23. W. Rapin, B. Bousquet, J. Lasue, P. Y. Meslin, J. L. Lacour, C. Fabre, A. Cousin, *Spectrochim. Acta B: At. Spectrosc.*, **137**, 13–22 (2017).
24. W. Wang, L. Sun, G. Wang, P. Zhang, L. Qi, L. Zheng, W. Dong, *J. Anal. At. Spectrom.*, **35**, No. 2, 357–365 (2020).
25. P. Chen, X. L. Wang, X. Hong, H. Wang, C. L. Zhao, Z. D. Jia, L. Zou, Y. M. Li, J. H. Fan, *Spectrosc. Spectr. Anal.*, **39**, No. 6, 1929 (2019).
26. F. Lisowski, E. Lisowski, *Appl. Sci.*, **10**, No. 14, 4717 (2020).
27. L. Yande, G. Xue, C. Mengjie, H. Zhaoguo, L. Xiaodong, Jia, *Laser Optoelectron. Prog.*, **57**, No. 9, 093006 (2020).
28. C. Yi, Y. Lv, H. Xiao, K. Ke, X. Yu, *Spectrochim. Acta B: At. Spectrosc.*, **138**, 72–80 (2017).
29. Y. W. Chu, S. S. Tang, S. X. Ma, Y. Y. Ma, Z. Q. Hao, Y. M. Guo, X. Y. Zeng, *Opt. Express*, **26**, No. 8, 10119–10127 (2018).
30. D. Syvilay, N. Wilkie-Chancellier, B. Trichereau, A. Texier, L. Martinez, S. Serfaty, V. Detalle, *Spectrochim. Acta B: At. Spectrosc.*, **114**, 38–45 (2015).
31. A. Ziegler, I. R. König, *Wiley Interdiscip. Rev. Data Min. Knowl. Discov.*, **4**, No. 1, 55–63 (2014).
32. P. Pořízka, J. Klus, A. Hrdlička, J. Vrábel, P. Škarková, D. Prochazka, J. Kaiser, *J. Anal. At. Spectrometry*, **32**, No. 2, 277–288 (2017).
33. J. P. Castro, E. R. Pereira-Filho, *J. Anal. At. Spectrometry*, **31**, No. 10, 2005–2014 (2016).